

December 2, 2024

LBNL-46980
hep-ph/0010231**On the Evolution of the Neutrino State inside the Sun**

Alexander Friedland

*Theoretical Physics Group**Ernest Orlando Lawrence Berkeley National Laboratory**University of California, Berkeley, California 94720*

and

*School of Natural Sciences, Institute for Advanced Study**Einstein Drive, Princeton, NJ 08540****Abstract**

We revisit several aspects of neutrino evolution in the Sun, motivated by our recent study of the so-called quasi-vacuum oscillation region. We point out that the traditional resonance condition can be used to describe the region in the Sun where the neutrino “jumps” between matter mass eigenstates only in the limit of small neutrino mixing angles $\theta \ll 1$. A modified condition is presented, which correctly gives the center of the “jumping” region for all values of θ , including $\theta > \pi/4$. An adiabaticity condition valid for all values of θ is also given. We investigate which part of the solar density profile is primarily responsible for matter effects in the quasi-vacuum oscillation regime. We present the results of numerical computations of the jumping probability P_c in a wide range of Δm^2 , interpolating between the vacuum oscillation region and the region where the standard exponential approximation is good, and present an empirical parametrization of these results in terms of elementary functions. Finally, we show how the known analytical results for the exponential, $1/x$, and linear matter distributions can be directly obtained from the formula for the hyperbolic tangent profile. We also give an explicit formula for the distribution $N_e \propto (\coth(x/l) \pm 1)$.

*New address from Sept. 1, 2000.

1 Introduction

The solar neutrino problem (SNP) is a discrepancy between the measured values of the solar neutrino flux at different energies [1, 2, 3, 4, 5] and the corresponding predictions of the Standard Solar Model (SSM) [6]. Not only is the observed flux suppressed, compared to the SSM predictions, but, if the data from the Homestake experiment are correct, the degree of suppression varies with energy. The leading explanation of this phenomenon is that neutrinos have small masses and the mass and flavor bases in the lepton sector are not aligned, just like in the quark sector. The resulting neutrino oscillations convert some of the solar electron neutrinos into another neutrino species.

Neutrino oscillation solutions to the SNP have traditionally been divided into the so-called Mikheyev-Smirnov-Wolfenstein (MSW) solutions [7, 8, 9] and the vacuum oscillation (VO) solutions, according to the physical mechanism responsible for the neutrino flavor conversion in each case. In the MSW case the conversion is caused by neutrino interactions with the solar (and Earth's) matter, while in the VO case it is due to long-wavelength neutrino oscillations in vacuum between the Sun and the Earth. Over time, it has become a tradition to treat the two cases completely separately, showing results in separate plots (see, for example, [10, 11]) and using different input formulas and different codes.

Recently, however, it has been pointed out by the author [12] that such a clear separation between the two regimes cannot be drawn, since matter effects for the vacuum oscillation solutions with $\Delta m^2 \gtrsim 5 \times 10^{-10} \text{ eV}^2$ are nonnegligible. This has subsequently been verified by other authors [13, 14, 15], and the term *quasi-vacuum oscillations* (QVO) has been coined to refer to the overlap region [13]. It is important to emphasize that the existence of a region where both vacuum oscillations and matter effects are important is not a trivial point, but a quantitative question, requiring an accurate analysis of the magnitude of the solar matter effects and the degree of decoherence of vacuum oscillations.

It is also worth mentioning that the experimental situation has since changed rather remarkably. The Super-Kamiokande spectrum data now disfavors a large fraction of the vacuum oscillation region with low Δm^2 (everything with $\Delta m^2 < 4 \times 10^{-10} \text{ eV}^2$) [16, 15]. The remaining portion of the VO solution is precisely where the solar matter effects affect the low energy pp flux in the gallium experiments, *i.e.*, the QVO solutions.

Prior to [12], the VO solutions had always been studied in the range of the neutrino mixing angle $0 \leq \theta \leq \pi/4$ for a fixed sign of Δm^2 . When matter effects are included, however, this only covers a half of the full parameter space. To cover the full space, one can either (i) keep θ in the range $0 \leq \theta \leq \pi/4$ and consider both signs of Δm^2 , or (ii) fix the sign of Δm^2 and vary θ from 0 to $\pi/2$. We advocate the second option as a better *physical* choice, because it makes manifest the continuity of physics around the maximal mixing [17, 18].

The parametrization $0 < \theta < \pi/2$ requires one to reexamine the choice of a variable for the plots, because the traditional variable $\sin^2 2\theta$ is not suitable for the purpose [17]. While θ or $\sin^2 \theta$ would both be adequate choices for plotting only the QVO region, they do not allow one to take a global view of the neutrino parameter space and show all solutions, including the SMA and (quasi)vacuum oscillation solutions, on the same plot [18]. A particularly convenient choice turns out to be $\tan^2 \theta$ on the logarithmic scale, first used in [19] to describe 3-family MSW oscillations. In addition to covering the range $0 < \theta < \pi/2$, it also does not introduce any unphysical singularity around $\theta = \pi/4$ (unlike the traditional $\sin^2 2\theta$, see [17]) and makes it easy to see where in the vacuum oscillation region the evolution in the Sun becomes completely nonadiabatic (points θ and $\pi/2 - \theta$ become equivalent, so that solutions become symmetric with respect to the $\theta = \pi/4$ line).

In this paper we address a series of theoretical questions that arise in the analysis of matter effects for $\theta \geq \pi/4$. Two such questions one has to face immediately when studying the QVO region are:

- What physical criteria are to be used in deciding whether the neutrino evolution is extremely nonadiabatic or whether matter effects modify the survival probability?
- At what radius in the Sun does the nonadiabatic “jumping” between the eigenstates of the instantaneous Hamiltonian take place?

The traditional wisdom is that one should analyze the density profile around the so-called resonance or level-crossing point, *i.e.*, the point where the separation between the eigenvalues of the instantaneous Hamiltonian is minimal and the local value of the mixing angle is $\theta_m = \pi/4$ (see, *e.g.*, [20, 21, 22, 23, 24, 25, 26]). This, however, clearly needs to be modified for large mixing angles. In particular, for $\theta > \pi/4$ the resonance, defined in this way, simply does not exist. On a more detailed level, one can ask

- What part of the solar electron density profile is mainly responsible for the matter effects in QVO?

Answering the last question is essential for properly interpreting the results of numerical computations in the QVO region. We will address these three questions in Section 2.

In Section 3 we present the results of numerical calculations of the neutrino jumping probability P_c in a wide range of Δm^2 and $\tan^2 \theta$, from the VO region to the region where the traditional exponential density approximation becomes valid. We also give a simple empirical prescription on how to compute matter effects in this range of the parameters in terms of only elementary functions. Such an empirical parametrization of numerical results can be helpful if one would like to be able to quickly estimate the value of P_c anywhere in the range in question without having to solve the differential equation each time.

Finally, in Section 4 we comment on the four known exact analytical solutions for the neutrino jumping probability P_c . In addition to the exponential distribution, explicit solutions have been given in the literature for the linear, $1/r$, and hyperbolic tangent matter profiles. One may wonder if these profiles have some features in common that make finding exact solutions possible. We point out that these results are not independent and that, given the formula for the tanh profile, one can very simply obtain the other three results. As an added benefit, we obtain an exact expression for the density distribution $N_e \propto (\coth(x/l) \pm 1)$.

2 Physical aspects of the nonadiabatic neutrino evolution

2.1 Review of the oscillation formalism

For completeness, we begin by summarizing the well-known basic formalism for neutrino propagation in matter. In the simplest case, when the mixing is between ν_e and another active neutrino species, the evolution of the neutrino state is determined by four parameters: the mass-squared splitting between the neutrino mass eigenstates $\Delta m^2 \equiv m_2^2 - m_1^2$, the neutrino mixing angle θ , the neutrino energy E_ν , and the electron number density N_e of the medium. One has to solve the Schrödinger equation $id\phi/dt = H\phi$ with the Hamiltonian

H given by [7]

$$H = \text{const} + \begin{pmatrix} A - \Delta \cos 2\theta & \Delta \sin 2\theta \\ \Delta \sin 2\theta & \Delta \cos 2\theta - A \end{pmatrix}. \quad (2.1)$$

Here $\Delta \equiv \Delta m^2/(4E_\nu)$, $A \equiv \sqrt{2}G_F N_e/2$, $\phi = (\phi_e, \phi_\mu)^T$ is the state vector made up of the electron neutrino and the muon neutrino.* The constant in the Hamiltonian is irrelevant for the study of oscillations and will be omitted from now on. The time variable t in the Schrödinger equation may be replaced by the distance traveled x , since solar neutrinos are ultrarelativistic.

For a constant electron number density N_e the Hamiltonian can be trivially diagonalized, $H' = VHV^\dagger = \text{diag}(-\Delta_m, +\Delta_m)$. The quantity Δ_m is given by a square root of the negative determinant of Eq. (2.1),

$$\Delta_m = \sqrt{(A - \Delta \cos 2\theta)^2 + (\Delta \sin 2\theta)^2} = \sqrt{A^2 - 2A\Delta \cos 2\theta + \Delta^2}. \quad (2.2)$$

In terms of Δ_m , the Hamiltonian (2.1) can be rewritten as

$$H = \begin{pmatrix} -\Delta_m \cos 2\theta_m & \Delta_m \sin 2\theta_m \\ \Delta_m \sin 2\theta_m & \Delta_m \cos 2\theta_m \end{pmatrix}, \quad (2.3)$$

where θ_m is the mixing angle in matter. The rotation matrix V is given by

$$V = \begin{pmatrix} \cos \theta_m & -\sin \theta_m \\ \sin \theta_m & \cos \theta_m \end{pmatrix}. \quad (2.4)$$

The parameters Δ_m and θ_m are related to the original parameters in the Hamiltonian (2.1) as follows

$$\Delta_m \sin 2\theta_m = \Delta \sin 2\theta, \quad (2.5)$$

$$\Delta_m \cos 2\theta_m = \Delta \cos 2\theta - A, \quad (2.6)$$

$$\tan 2\theta_m = \frac{\Delta \sin 2\theta}{\Delta \cos 2\theta - A}. \quad (2.7)$$

We will always label the light mass eigenstate as ν_1 and the heavy one as ν_2 . Since one can redefine the phases of $\nu_{e,\mu}$ and $\nu_{1,2}$, it is easy to see that in this convention the physical range of the mixing angle is $0 \leq \theta \leq \pi/2$ [18, 17].

*In reality, ϕ_μ here denotes a linear combination of ϕ_μ and ϕ_τ in which ϕ_e oscillates.

The time evolution of the mass eigenstates is particularly simple. Each of the two mass eigenstates evolves only by a phase, *i.e.*, for $N_e(x) = \text{const}$ we have $|\nu_1(t)\rangle = |\nu_1(0)\rangle \exp(i\Delta_m t)$, $|\nu_2(t)\rangle = |\nu_2(0)\rangle \exp(-i\Delta_m t)$. If at time $t = 0$ a state is a linear combination of $a|\nu_1(0)\rangle + |\nu_2(0)\rangle$, the absolute values of the coefficients a and b do not change with time, *i.e.*, the probability of the neutrino “jumping” from one Hamiltonian eigenstate to another is zero. This remains true when the density of electrons varies very slowly, so that the eigenstates of the instantaneous Hamiltonian change slowly along the neutrino trajectory. Such a case is referred to as the *adiabatic* evolution. In the following we will refer to the eigenstates of the instantaneous Hamiltonian as the matter mass eigenstates.

At the same time it is obvious that if the density of electrons changes sufficiently quickly the jumping probability P_c between the matter mass eigenstates will be nonzero. In the extreme case when the density changes abruptly from one value to another, the flavor state does not have any time to evolve, while the mass basis in matter instantaneously rotates. It is easy to see that the jumping probability in this situation is given by

$$P_c^{\text{NA}} = \sin^2(\theta^{\text{before}} - \theta^{\text{after}}). \quad (2.8)$$

In general, for a monotonically varying density P_c lies between 0 and P_c^{NA} .

In this paper we are primarily concerned with physics affecting the jumping probability for solar neutrinos. The electron number density inside the Sun, N_e , falls off as a function of the distance from the center r , as shown in Fig. 1 [6]. In the range $0.15R_\odot \lesssim r \lesssim 0.65R_\odot$ the profile can be approximated very well by an exponential $N_e(r) \propto \exp(-r/r_0)$, with $r_0 = R_\odot/10.54 = 6.60 \times 10^4$ km (shown by a straight line in the Figure). However, in the outer layers of the Sun (and also in the core) the profile deviates significantly from the exponential.

Although in the case of a varying density the Hamiltonian in general cannot be diagonalized, in order to study the jumping probability between the matter mass eigenstates it is still convenient to use the basis these states define. Substituting in the Schrödinger equation $\phi = V^\dagger \psi$, we get

$$\begin{aligned} i \frac{d}{dx} (V^\dagger \psi) &= H V^\dagger \psi, \\ i \frac{\partial \psi}{\partial x} &= V H V^\dagger \psi - i V \frac{\partial V^\dagger}{\partial x} \psi. \end{aligned} \quad (2.9)$$

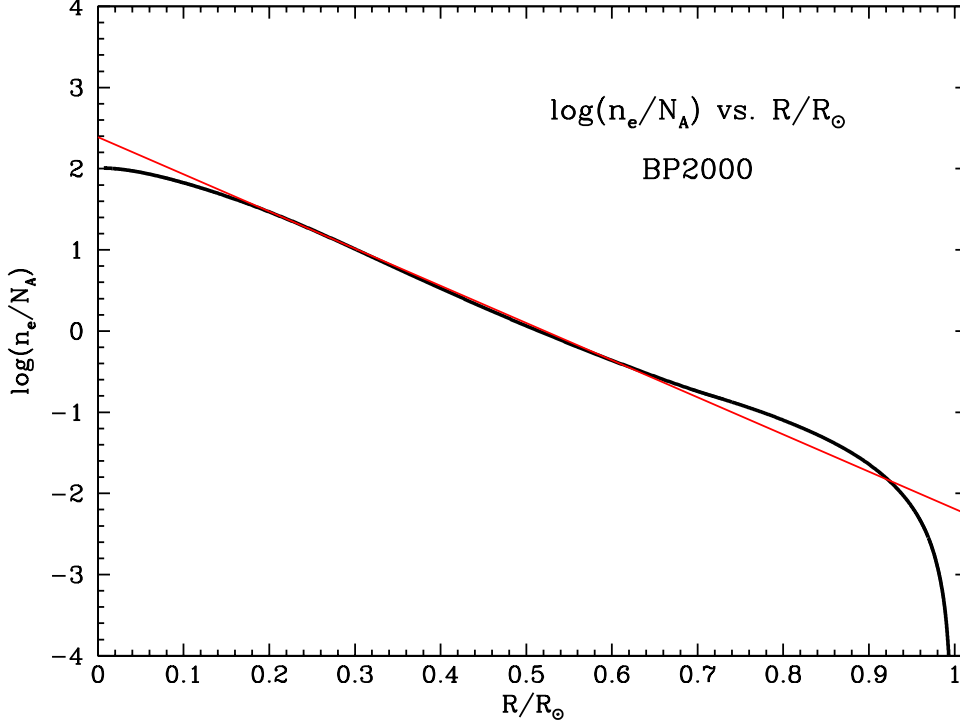


Figure 1: The electron number density profile of the Sun according to the BP2000 standard solar model.

Since $VHV^\dagger = \text{diag}(-\Delta_m, +\Delta_m)$ and from Eq. (2.4)

$$V \frac{dV^\dagger}{dx} = \begin{pmatrix} 0 & 1 \\ -1 & 0 \end{pmatrix} \frac{d\theta_m}{dx},$$

we obtain the evolution equation in the basis of the matter mass eigenstates [20]

$$\frac{d}{dx} \begin{pmatrix} \psi_1 \\ \psi_2 \end{pmatrix} = \begin{pmatrix} i\Delta_m & -d\theta_m/dx \\ d\theta_m/dx & -i\Delta_m \end{pmatrix} \begin{pmatrix} \psi_1 \\ \psi_2 \end{pmatrix}. \quad (2.10)$$

We will find it helpful to choose θ_m instead of x as an independent variable. So long as the density varies monotonically, such a change is one-to-one.

Eq. (2.10) becomes

$$\frac{d}{d\theta_m} \begin{pmatrix} \psi_1 \\ \psi_2 \end{pmatrix} = \begin{pmatrix} i\Delta_m/\dot{\theta}_m & -1 \\ 1 & -i\Delta_m/\dot{\theta}_m \end{pmatrix} \begin{pmatrix} \psi_1 \\ \psi_2 \end{pmatrix}, \quad (2.11)$$

Here Δ_m and $\dot{\theta}_m \equiv d\theta_m/dx$ can both be expressed in terms of θ_m using the following relationships

$$\dot{\theta}_m = \frac{\sin^2 2\theta_m}{2\Delta \sin 2\theta} \frac{dA}{dx}, \quad (2.12)$$

$$\frac{\Delta_m}{\dot{\theta}_m} = \frac{2\Delta^2 \sin^2 2\theta}{\sin^3 2\theta_m} \frac{1}{dA/dx}, \quad (2.13)$$

$$A = \frac{\Delta \sin(2\theta_m - 2\theta)}{\sin 2\theta_m}, \quad (2.14)$$

which follow directly from Eqs. (2.5-2.7). For instance, for the idealized exponential profile $A(x) = A_0 \exp(-x/r_0)$ the derivative is $dA(x)/dx = -A(x)/r_0$ and so

$$\frac{\Delta_m}{\dot{\theta}_m} = -\frac{2\Delta r_0 \sin^2 2\theta}{\sin^2 2\theta_m \sin(2\theta_m - 2\theta)}. \quad (2.15)$$

The angle θ_m varies from its value at the production point θ_\odot to its vacuum value θ . For the infinite exponential profile we have $\theta_\odot \rightarrow \pi/2$. Notice that the quantity $\Delta_m/\dot{\theta}_m$ in Eq. (2.15) is singular when θ_m approaches either of its limiting values, as should be expected.

The shape of the function $|\Delta_m/\dot{\theta}_m|$ for $\theta = \pi/4$ and $\Delta = 10^{-9} \text{ eV}^2/\text{MeV}$ for the idealized exponential profile is illustrated in Fig. 2 by the solid curve. The value of r_0 was chosen to be $R_\odot/10.54$ (according to the slope of the best fit line in Fig. 1). The dashed curve in the Figure shows the same quantity for the realistic BP2000 solar profile. It is important to keep in mind that the two curves change qualitatively differently as one changes Δ . While the exponential curve just scales by an overall factor, the BP2000 curve also changes its shape, approaching that of the shape of the (rescaled) solid curve for sufficiently large values of Δ .

Eq. (2.11) is a convenient starting point for our analysis. If for almost the entire interval between θ and θ_\odot the condition $|\Delta_m/\dot{\theta}_m||\psi_1| \ll |\psi_2|$ is satisfied, the diagonal terms can be neglected and

$$\psi(\theta) = \exp \left[\int_{\theta_\odot}^{\theta} d\theta_m \begin{pmatrix} 0 & -1 \\ 1 & 0 \end{pmatrix} \right] \psi(\theta_\odot)$$

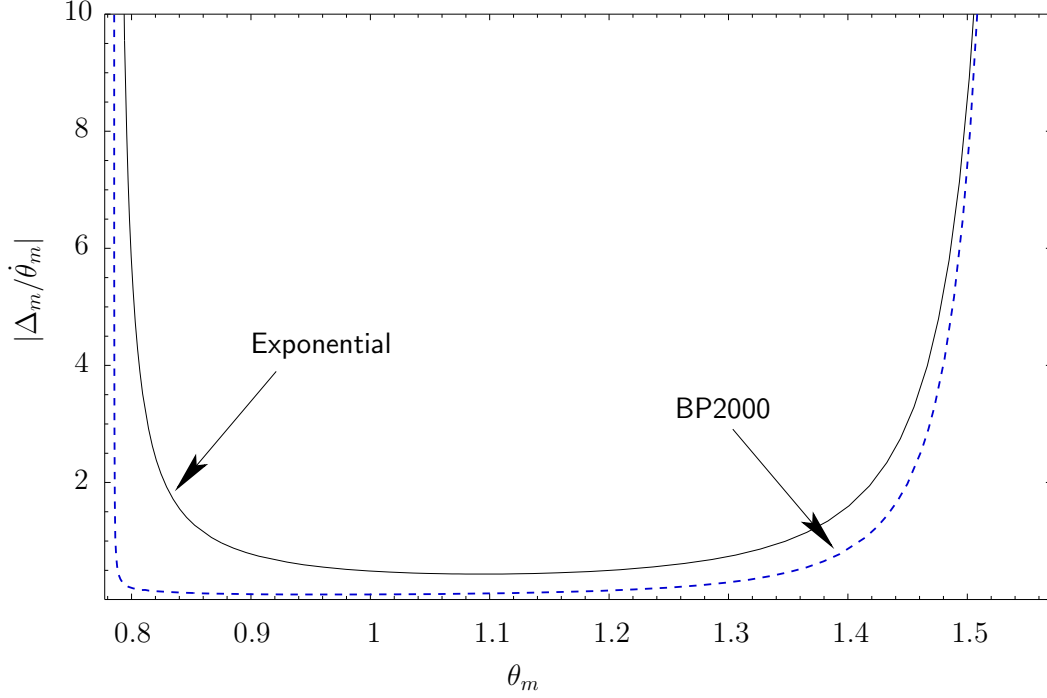


Figure 2: The quantity $|\Delta_m/\dot{\theta}_m|$ as a function of θ_m for the exponential profile $A(x) \propto \exp(-x/r_0)$ (solid line) and BP2000 solar profile (dashed line) for $\theta = \pi/4$, $\Delta = 10^{-9}$ eV²/MeV.

$$= \begin{pmatrix} \cos(\theta - \theta_\odot) & -\sin(\theta - \theta_\odot) \\ \sin(\theta - \theta_\odot) & \cos(\theta - \theta_\odot) \end{pmatrix} \psi(\theta_\odot), \quad (2.16)$$

so the jumping probability is given by Eq. (2.8), as expected. In the opposite limit $|\Delta_m/\dot{\theta}_m||\psi_1| \gg |\psi_2|$ the off-diagonal terms can be neglected, giving us the adiabatic case. Before discussing the adiabaticity conditions any further, however, we would like to address the question at what radius in the Sun the jumping between the matter mass eigenstates takes place.

2.2 Modification of the notion of resonance for large θ .

Conventional wisdom dictates that the adiabaticity condition is violated maximally at the resonance point

$$A = \Delta \cos 2\theta, \quad (2.17)$$

where the separation between the energy levels is minimal and $\theta_m = \pi/4$. This assertion can be found in the original works [21, 22, 20, 27], as well as in numerous subsequent reviews on the subject, *e. g.* [24, 25, 26]. However, in all these papers it is assumed either explicitly or implicitly that the vacuum mixing angle θ is small. It is easy to see that for a large value of the mixing angle the condition of Eq. (2.17) leads to a contradiction.

For small θ , Eq. (2.17) is satisfied in some layer in the Sun where the density is $A(x) \simeq \Delta$. As the value of θ increases, however, (2.17) predicts that the resonance occurs at lower and lower electron density until, as θ approaches $\pi/4$, it moves off to infinity. It is physically clear that no level jumping can occur at infinity where neutrinos undergo ordinary vacuum oscillations. The problem is even more obvious when $\theta > \pi/4$, in which case the resonance simply never occurs. At the same time, it is also clear, at least in the extreme nonadiabatic regime, that the level jumping probability is nonzero for *any* value of θ and varies *smoothly* around $\theta = \pi/4$, $P_c = \sin^2(\pi/2 - \theta) = \cos^2 \theta$.

The resolution to this apparent paradox is very simple. As Eq. (2.11) suggests, the adiabaticity is maximally violated at the minimum of $|\Delta_m/\dot{\theta}_m|$ ([20, 27]). However, it is easy to see that the minimum of $|\Delta_m/\dot{\theta}_m|$ in general does not reduce to the condition of Eq. (2.17). This can be illustrated on the example of the infinite exponential density distribution. Differentiating Eq. (2.15), one finds that the minimum occurs when

$$\cot(2\theta_m - 2\theta) + 2 \cot(2\theta_m) = 0, \quad (2.18)$$

or

$$A = \Delta \frac{\cos 2\theta + \sqrt{8 + \cos^2 2\theta}}{4}. \quad (2.19)$$

Unlike Eq. (2.17), Eq. (2.19) states there is a nonadiabatic part of the neutrino trajectory for all physical values of θ , including $\theta \geq \pi/4$. While both equations for small θ predict that jumping between the local mass eigenstates will occur around $A = \Delta$, Eq. (2.19) states that for maximal mixing it will occur around $A = \Delta/\sqrt{2}$, not at infinity, and for $\theta \rightarrow \pi/2$ Eq. (2.19) gives $A \rightarrow \Delta/2$, all physically reasonable results.

To understand this behavior, notice that $\dot{\theta}_m$ has a maximum at

$$\theta_m = \pi/4 + \theta/2, \quad (2.20)$$

which corresponds to $A = \Delta$, but, because Δ_m decreases with x , the minimum of $\Delta_m/\dot{\theta}_m$ occurs at somewhat smaller A . Condition (2.20) can be

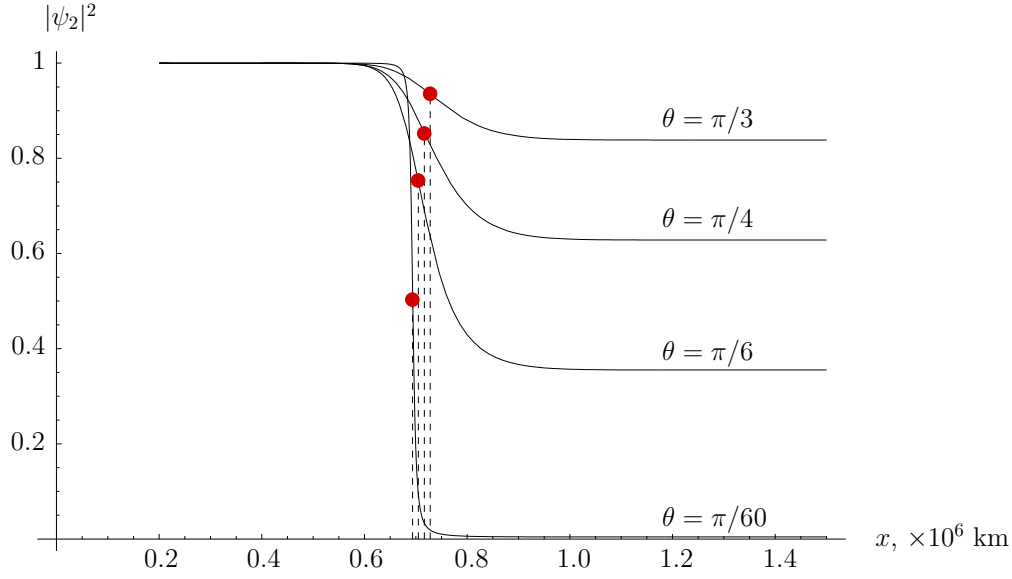


Figure 3: Neutrino state evolution in the case of an idealized infinite exponential density profile for $\Delta m^2/E_\nu = 10^{-9}$ eV²/MeV. The plot shows the probability of finding the neutrino in the heavy matter mass eigenstate ν_2 as a function of position x for four different values of the vacuum mixing angle. The points of the maximal violation of the adiabaticity condition, as predicted by Eq. (2.19), are marked.

viewed as the point where the flavor composition of the neutrino states changes the fastest. Thus, Eq. (2.17) not only does not describe the point of the maximal violation of the adiabaticity for large values of θ , but it also does not specify the point where the flavor conversion occurs at the maximal rate in that case.

Note also that Eqs. (2.17) and (2.19) have different Taylor series expansion around $\theta = 0$,

$$\begin{aligned} A &\simeq \Delta(1 - 2\theta^2/3) && \text{for Eq. (2.19),} \\ A &\simeq \Delta(1 - 2\theta^2) && \text{for Eq. (2.17).} \end{aligned}$$

Thus, Eq. (2.17) fails to predict how the point of maximal nonadiabaticity *shifts* as a function of θ even at small θ .

The situation is illustrated in Fig. 3, which shows the probability of finding the neutrino in the heavy mass state ν_2 as a function of the distance

x. The parameters of the exponential were taken from the fit line of Fig. 1 and $\Delta m^2/E_\nu = 10^{-9} \text{ eV}^2/\text{MeV}$. Three large values of the mixing angle ($\theta = \pi/6, \pi/4$, and $\pi/3$) and one small value ($\theta = \pi/60$) were chosen. The dashed lines and dots mark the points where the adiabaticity condition is maximally violated, as predicted by Eq. (2.19). One can see that the transitions between the Hamiltonian states in all four cases indeed occur around the marked points.

The belief that jumping between the matter mass eigenstates occurs at the resonance for all angles might have been one of the reasons for the tradition to treat separately the cases of $\theta < \pi/4$ and $\theta > \pi/4$, obscuring the fact that the physics is completely continuous across the maximal mixing. Over the years, it has caused some unfortunate confusions, as exemplified by the flawed criticism of the results of [12] in [28]. It was probably the principal reason why the correct expression for the electron neutrino survival probability in the $\theta > \pi/4$ part of the QVO region was not given until recently [17, 12] (*c.f.* Eq. (6) in [19] where, in the context of 3-family MSW oscillations, the full range $0 \leq \theta \leq \pi/2$ was first correctly considered).

One important application of Eq. (2.19) is the determination of the phase of vacuum oscillations on the Earth [29, 30]. It has been known since [7] that neutrinos with low Δ practically do not oscillate in the solar core, where $A \gg \Delta$. If the jumping between matter mass eigenstates indeed occurs at the resonance (2.17), one would expect that in the canonical vacuum oscillation formula

$$P = 1 - \sin^2 2\theta \sin^2 \left(1.27 \frac{\Delta m^2 L}{E} + \delta_{\text{res}} \right), \quad (2.21)$$

the residual phase δ_{res} is minimized when the distance L is measured from the resonance. Ref. [29] indeed begins with this assumption, but after discussing the resulting formulas notes that the residual phase is much smaller if L is instead measured from the layer where $A = \Delta$, not $A = \Delta \cos 2\theta$. It is unfortunate that this important observation has not received proper attention and was not further developed in the subsequent literature. Eq. (2.19) shows that this result is not just a mathematical coincidence, but has a simple physical explanation.

Finally, it is important to establish at what density the jumping occurs in the case of the realistic solar profile. Qualitatively, it is not difficult to anticipate the changes to Eq. (2.19) in this case.

- For sufficiently large Δ , the jumping occurs entirely within the exponential part of the profile, so that Eq. (2.19) directly applies.
- For small Δ , the nonadiabatic region will lie in the outer solar layers where the profile falls off rather rapidly. While for small θ the minimum of $\Delta_m/\dot{\theta}_m$ should still, of course, occur at $A = \Delta$, for large angles it is shifted to values of A somewhat lower than that predicted by Eq. (2.19).
- For Δ in the intermediate range, the jumping occurs in the part of the profile where the density falls off somewhat slower than in the exponential part. There the value of the ratio A/Δ at large θ should increase compared to Eq. (2.19).

These qualitative expectations are supported by the results of numerical calculations presented in Fig. 4, where the ratio A/Δ at the point of minimal $\Delta_m/\dot{\theta}_m$ is plotted as function of θ . The three curves shown correspond to the values of Δ in the three different regimes ($\Delta = 2 \times 10^{-6}$ eV²/MeV (curve 1), $\Delta = 7 \times 10^{-7}$ eV²/MeV (curve 2), and $\Delta = 1 \times 10^{-8}$ eV²/MeV (curve 3)).

2.3 Adiabaticity condition for large θ .

Our goal next is to formulate the criterion for the breakdown of adiabaticity that can be applied to all, and not just small, values of θ . As previously mentioned, the evolution is nonadiabatic if $|\Delta_m/\dot{\theta}_m||\psi_1| \ll |\psi_2|$. Recalling that in the nonadiabatic case $|\psi_1| \simeq \cos \theta_m$, $|\psi_2| \simeq \sin \theta_m$, we can write the nonadiabaticity condition as

$$|\Delta_m/\dot{\theta}_m|^{\min} \ll \tan \theta_m^{\min}. \quad (2.22)$$

Eq. (2.22) is to be compared with the commonly cited condition [20]

$$|\Delta_m/\dot{\theta}_m|^{\min} \ll 1. \quad (2.23)$$

The two clearly agree in the limit of small θ . For $\theta \gtrsim \pi/4$, however, the two conditions are different and it can be verified that Eq. (2.22) is the correct one.

This can be demonstrated on the example of the exponential profile. In this case an exact analytical solution is known [31, 32]:

$$P_c = \frac{e^{\gamma \cos^2 \theta} - 1}{e^\gamma - 1}. \quad (2.24)$$

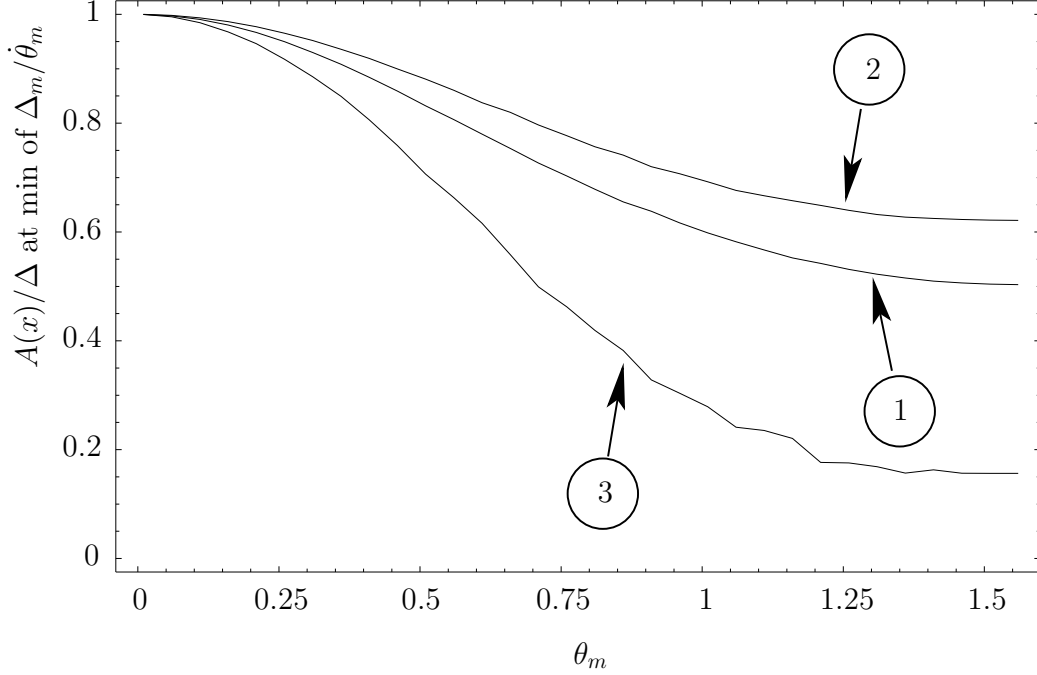


Figure 4: The value of the ratio $A(x)/\Delta$ at the minimum of $\Delta_m/\dot{\theta}_m$ computed for the realistic solar density profile (BP2000). The curves correspond to $\Delta = 2 \times 10^{-6}$ eV²/MeV (curve 1), $\Delta = 7 \times 10^{-7}$ eV²/MeV (curve 2), and $\Delta = 1 \times 10^{-8}$ eV²/MeV (curve 3).

Eq. (2.24) has two regimes. For small mixing angles, the formula reduces to $P_c = \exp(-\gamma \sin^2 \theta)$, and so the evolution is nonadiabatic when $\gamma \theta^2 = 4\pi r_0 \Delta \theta^2 \ll 1$. By contrast, for large mixing angles the situation is different. For $\theta \gtrsim \pi/4$ and $\gamma \gg 1$ the numerator is always much smaller than the denominator. The transition between the adiabatic and nonadiabatic regimes thus occurs when $\gamma \sim 1$, with a weak dependence on θ .

Let us see if Eq. (2.22) correctly captures this behavior. For simplification, we will take $\theta_m^{\min} \approx \pi/4 + \theta/2$ (corresponding to the maximum of $\dot{\theta}_m$, Eq. (2.20)). Eq. (2.22) in this case becomes

$$8\Delta r_0 \frac{\sin \theta \tan \theta}{\tan(\pi/4 + \theta/2)} \ll 1. \quad (2.25)$$

Fig. 5 shows the contour of $8\Delta r_0 \sin \theta \tan \theta / \tan(\pi/4 + \theta/2) = 0.5$, computed

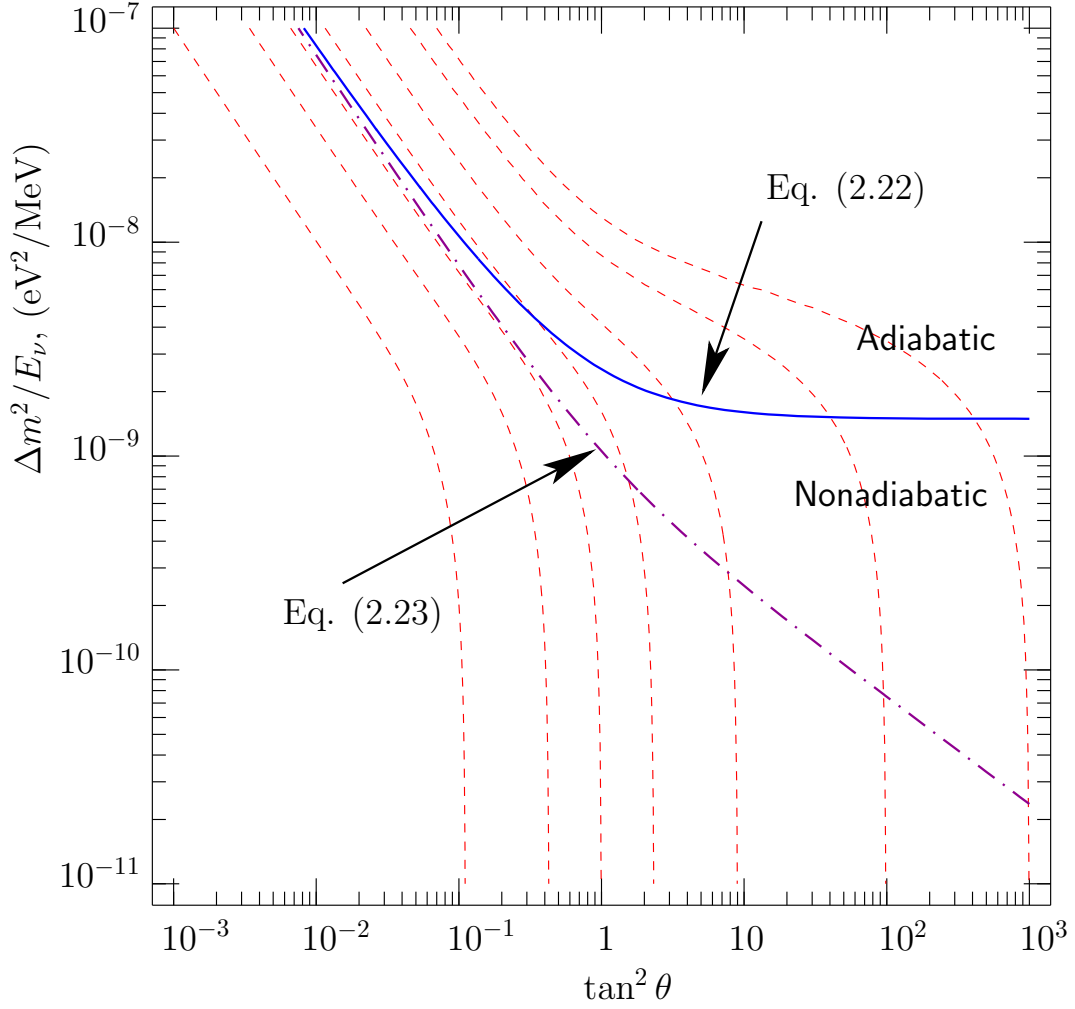


Figure 5: The boundary between the adiabatic and nonadiabatic regions in the case of the exponential profile according to Eq. (2.22) (solid curve) and Eq. (2.23) (dash-dotted curve). The dashed curves show the contours of constant P_c . For large angles Eq. (2.22) provides a better description of the boundary.

for the best fit exponential to the BP2000 density profile (solid line). For comparison, the dash-dotted curve shows the prediction of Eq. (2.23). The dashed curves show contours of constant P_c computed with Eq. (2.24). It is clear from the Figure that the description of Eq. (2.22) is correct not only for small θ , but also for $\theta \gtrsim \pi/4$. The transition from adiabaticity to nonadiabaticity for $\theta \gtrsim \pi/4$ occurs for $\Delta m^2/E_\nu \sim 10^{-9}$ eV²/MeV, precisely where $\gamma \sim 1$.

Eq. (2.22) can also be applied to describe the boundary between the adiabatic and nonadiabatic region in the case of the realistic solar profile. It turns out that the shape of the boundary in this case is similar to that for the exponential density profile. The corresponding numerical results will be presented in Sect. 3, after we consider in detail how one can understand matter effects on the boundary between the adiabatic and nonadiabatic regions (QVO) for the realistic BP2000 profile.

2.4 Matter effects in the QVO region.

In this subsection we investigate which part of the solar profile is primarily responsible for the initial deviation of P_c from $\cos^2 \theta$ in the QVO regime. Superficially, it may seem that for $\Delta m^2/E_\nu \sim 10^{-9}$ eV²/MeV the neutrino evolution should be completely nonadiabatic. Indeed, the condition $A \simeq \Delta$ in this case is satisfied very close to the Sun's edge (at $x = 6.9 \times 10^5$ km for the exponential profile and $x = 6.6 \times 10^5$ km for the BP2000 profile), where the electron number density falls off very rapidly. Such naive analysis is, however, incorrect. Numerical calculations [12, 13, 14] show that the solar matter effects in this range of $\Delta m^2/E_\nu$ do cause a significant deviation from the extreme nonadiabatic limit. In fact, for $\Delta m^2/E_\nu \lesssim 5 \times 10^{-9}$ the numerical results can be described well by Eq. (2.24) with $r_0 = R_\odot/18.4$, as shown in [12]. Our task next is to understand the physics behind this phenomenon.

We start by noticing that in the case of the exponential profile an important role is played by the parts of the trajectory where θ_m is close to either $\pi/2$ or θ , because there the combination $\Delta_m/\dot{\theta}_m$ is large (see Fig. 2). Even if around the point of minimum of $|\Delta_m/\dot{\theta}_m|$ the evolution approaches extreme nonadiabatic, the effects around the poles of $\Delta_m/\dot{\theta}_m$ cannot be ignored. Moreover, because the function in Eq. (2.15) has a *double* pole at $\theta_m = \pi/2$, the region around $\pi/2$ plays a relatively more important role in causing deviations from the extreme nonadiabatic regime than the region

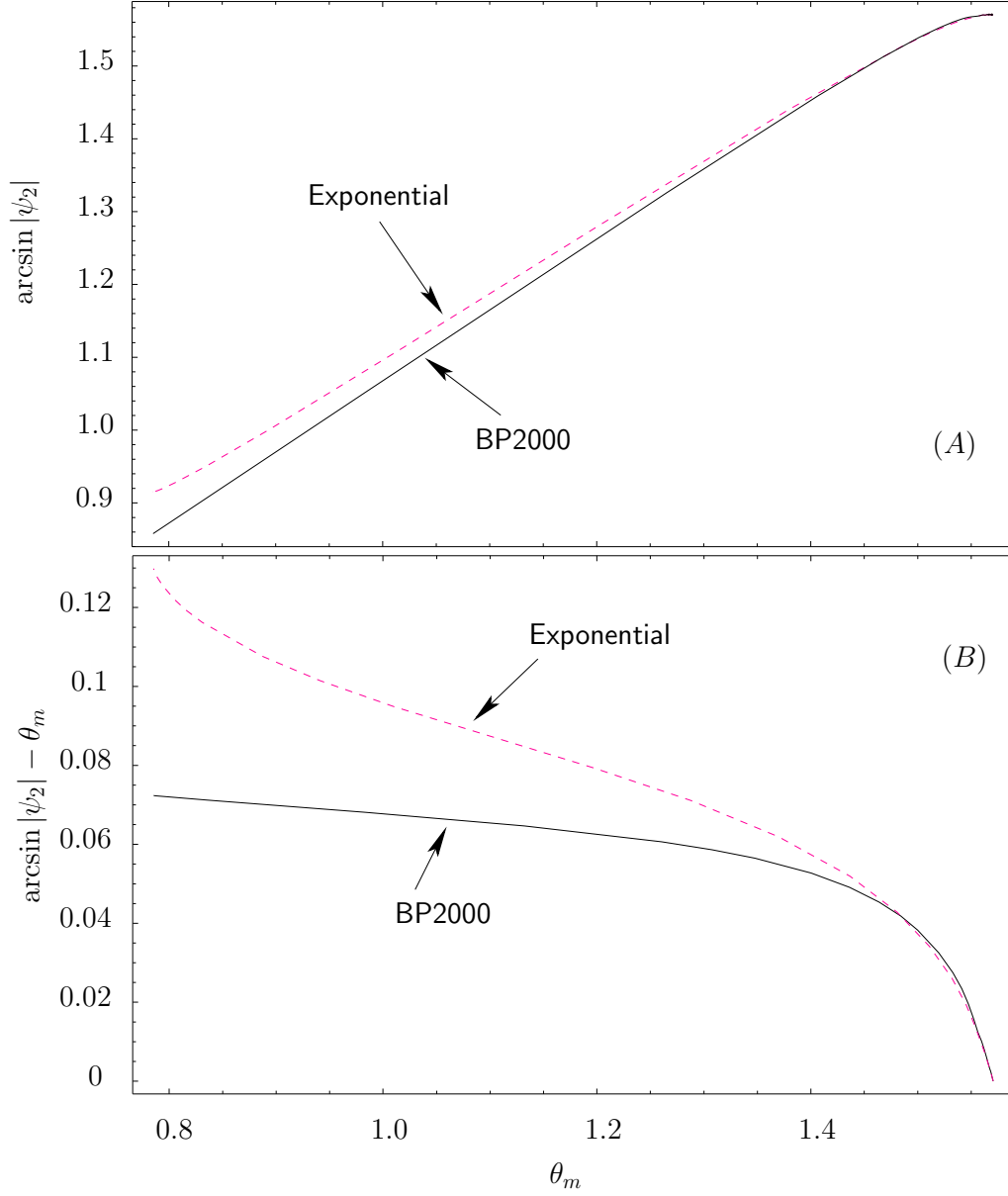


Figure 6: The comparison of the neutrino state evolution in the infinite exponential profile (dashed) and the realistic solar profile according to the BP2000 solar model (solid), plotted as a function of the mixing angle in matter θ_m . The bottom figure shows the deviation of the evolution in both cases from extreme nonadiabatic.

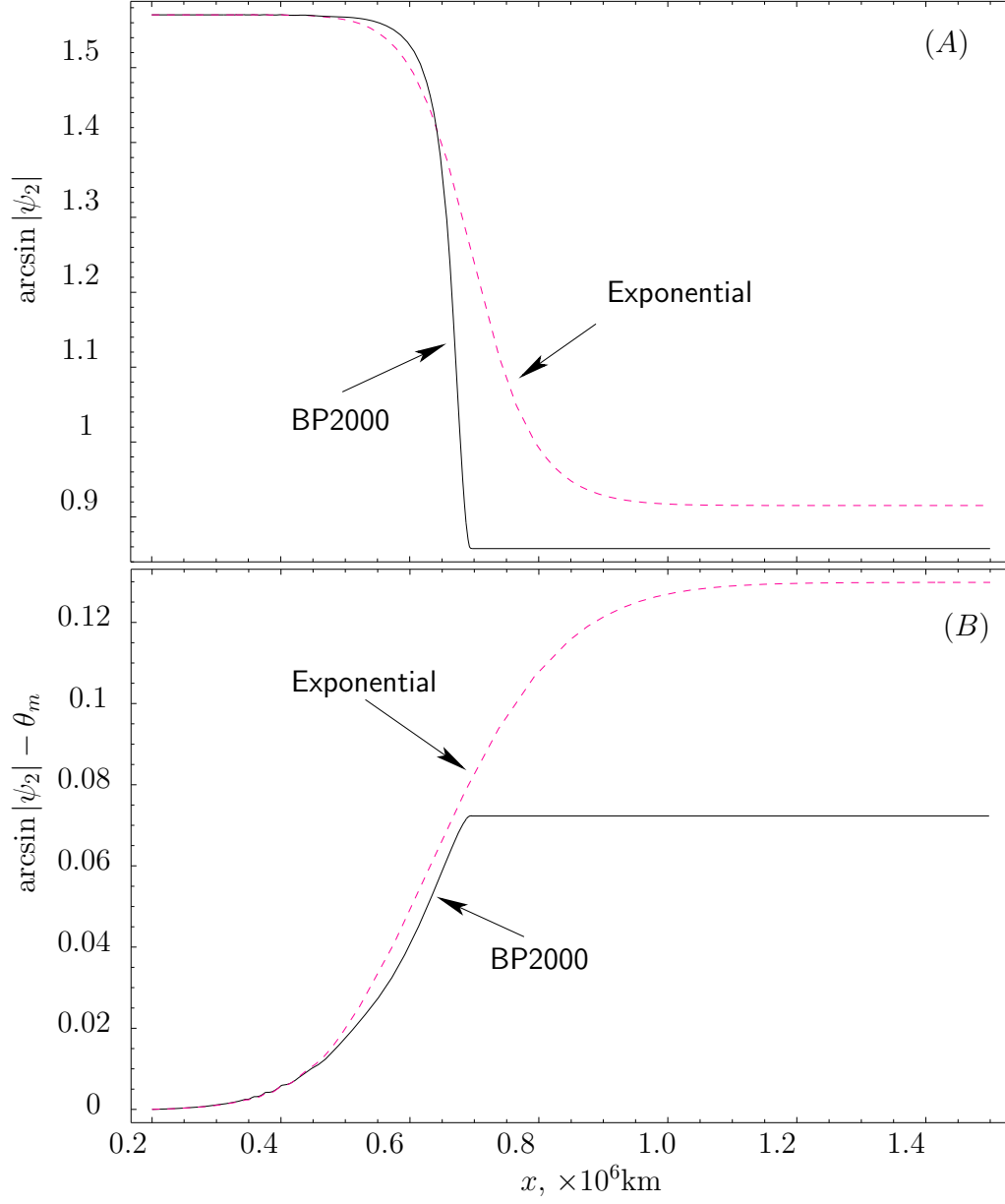


Figure 7: The same as Fig. 6, but as a function of the distance from the center of the Sun x .

around θ .

In going from the infinite exponential profile to the realistic solar density profile one truncates the part of the profile around $A(x) \sim \Delta$ and beyond. The part around the double pole, however, is not very different in the two cases (see Fig. 2). This part of the density profile still contributes to make the evolution partially adiabatic.

One way to illustrate this is by showing how $|\psi_2(\theta_m)|$ deviates from its extreme nonadiabatic dependence $|\psi_2(\theta_m)| = \sin \theta_m$. Fig. 6(A) shows the probability of finding the neutrino in the heavy adiabatic eigenstate as a function of the mixing angle in matter θ_m for $\Delta m^2/E_\nu = 10^{-9}$ eV²/MeV, $\theta = \pi/4$. Results for both the infinite exponential and the BP2000 profiles are shown. Fig. 6(B) shows the graph of $\Delta\theta_m \equiv \arcsin |\psi_2(\theta_m)| - \theta_m$ as a function of θ_m . The main contribution to $\Delta\theta_m$ comes from the region $1.4 \lesssim \theta_m < \pi/2$, where the profile is close to the exponential.

Fig. 7 shows the same evolution in the physical x -space. It shows that most of the contribution to $\Delta\theta_m$ comes from the part of the profile between $0.7R_\odot$ and R_\odot . It would thus be incorrect to try to estimate $\Delta\theta_m$ by computing the slope around the point $A = \Delta$, since for large θ the entire region $x \gtrsim 0.7R_\odot$ is important.

3 Numerical studies of P_c using BP2000 solar profile

In this Section we present the results of accurate numerical computations of the jumping probability P_c in the realistic (BP2000) solar density profile. It is easy to anticipate what these results should be in two limiting regimes. For sufficiently large $\Delta m^2/E_\nu$ the condition of Eq. (2.19) is satisfied well inside the Sun, where the profile is exponential with $r_0 = R_\odot/10.54$. Hence, above some value of $\Delta m^2/E_\nu$ the jumping probability should be adequately described by Eq. (2.24). On the other hand, as shown in [12], for $\Delta m^2/E_\nu \lesssim 5 \times 10^{-9}$ Eq. (2.24) provides a good fit to numerical results, provided one takes $r_0 = R_\odot/18.4$. We next present numerical results for P_c that cover the entire range between these two regimes.

We numerically solve Eq. (2.10) on a grid of points in the range $10^{-3} < \tan^2 \theta < 10$, 10^{-11} eV²/MeV $< \Delta m^2/E_\nu < 2 \times 10^{-7}$ eV²/MeV. The resulting contours of constant P_c are shown in Fig. 8 by solid curves.

It is easy to interpret the shape of the contours for $\theta \ll 1$. In this case the standard resonance description applies and, importantly, the resonance is very narrow. As a result, the jumping probability can be adequately described by the analytical result for a linear density profile, $P_c \rightarrow \exp(-\pi\Delta^2|dA(x)/dx|_{\text{res}}^{-1}\sin^2 2\theta)$ (see Eq. (4.28) of Sect. 4)*. One can indeed see that the contours in Fig. 8 for small θ follow the behavior of the changing slope of the BP2000 density profile in Fig. 1.

For large θ and low Δ this description, as discussed in Sect. 2.4, is no longer valid, since the nonadiabatic region is wide and part of it is cut off by the sharp density drop near the solar edge. Instead, as already mentioned, in this region one can use Eq. (2.24) with $r_0 = R_\odot/18.4$.

For practical calculations it is convenient to have a simple expression involving only elementary functions that provides a satisfactory means of estimating P_c without having to solve the differential equation each time. We can construct such a purely empirical fit function by taking Eq. (2.24) as a starting point. Since for both large and small values of $\Delta m^2/E_\nu$ one can use Eq. (2.24) with the appropriate values of r_0 , we can modify Eq. (2.24) by making r_0 a function of $\Delta m^2/E_\nu$, smoothly interpolating between $R_\odot/10.54$ and $R_\odot/18.4$,

$$r_0(\Delta m^2/E_\nu) = \frac{R_\odot}{10.54} \left[0.75 \left(\frac{1}{\pi} \arctan[-10(a+8)] + \frac{1}{2} \right) + 1 \right]^{-1}, \quad (3.26)$$

where $a = \log_{10}[(\Delta m^2/E_\nu)/(\text{eV}^2/\text{MeV})]$. This provides an adequate fit for both $\Delta m^2/E_\nu \lesssim 5 \times 10^{-9} \text{ eV}^2/\text{MeV}$ and $\Delta m^2/E_\nu \gtrsim 10^{-7} \text{ eV}^2/\text{MeV}$. By making additional modifications to the function it is possible to obtain a reasonable fit also to the contours in the intermediate region,

$$\begin{aligned} r_0^{\text{fit}}(\Delta m^2/E_\nu) &= \frac{R_\odot}{10.54} \left[0.75 \left(\frac{1}{\pi} \arctan[-10(a+7.95) + 0.9b] + \frac{1}{2} \right) \right. \\ &\quad \left. - 0.3 \exp \left(-\frac{(a+7.7)^2}{0.5^2} \right) + 1 \right]^{-1}, \end{aligned} \quad (3.27)$$

where $b = \log_{10}[\tan^2 \theta]$. It is important to emphasize that this equation should only be viewed as a purely empirical fit to the numerical results, intended to facilitate practical computations of the solar neutrino survival probability.

*This is the physical reason why the formula for the exponential distribution, Eq. (2.24), in the limit of small θ reduces to the linear result.

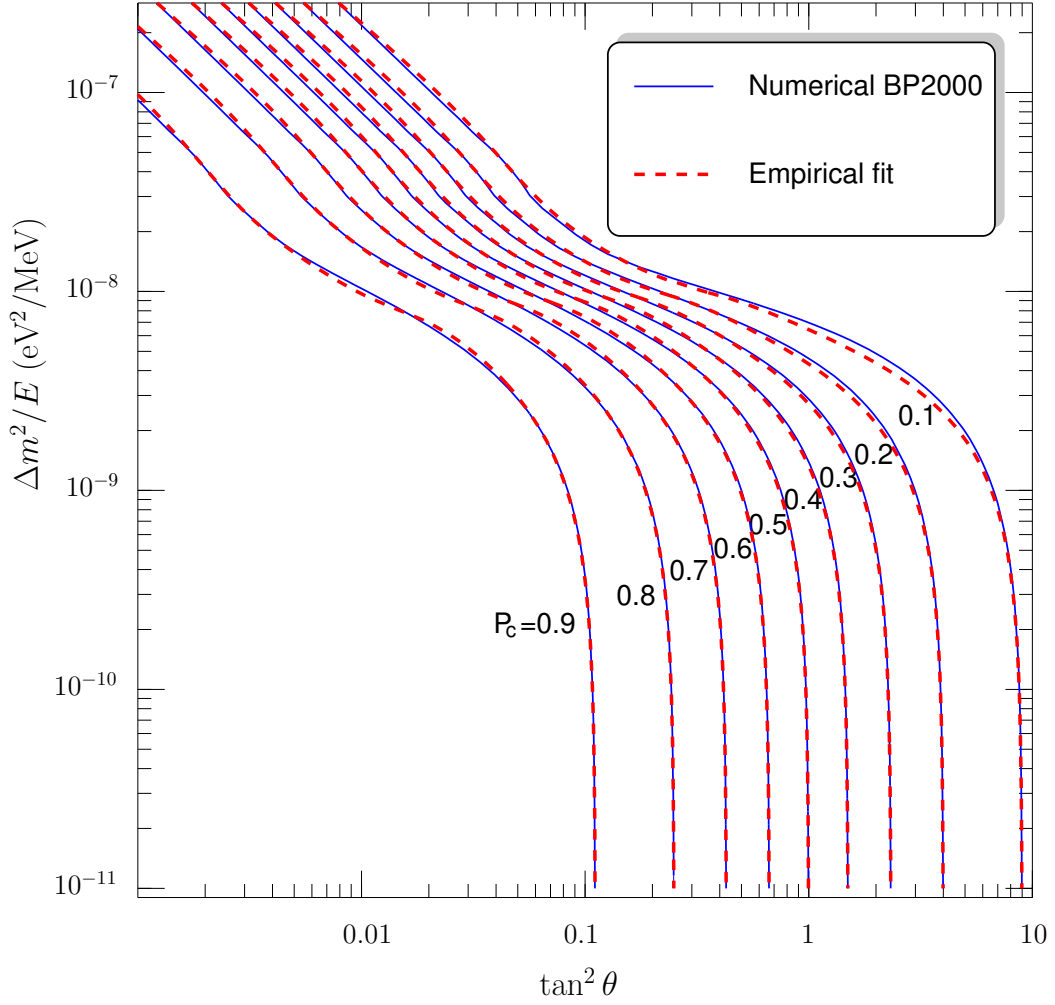


Figure 8: Contours of constant level jumping probability P_c . The solid line represent the result of numerical calculations using the BP2000 solar profile. The dashed lines illustrate a possible empirical fit using only elementary functions (Eq. (3.26)).

The contours of constant P_c^{fit} computed with Eq. (3.27) are shown by dashed lines in Fig. 8. The discrepancy between the BP2000 numerical results and P_c^{fit} is $|P_c^{\text{fit}} - P_c^{\text{BP2000}}| < 0.022$.

4 All known solutions can be derived from the one for the tanh profile.

In general, there are very few profiles for which exact analytical solutions are known. In addition to the exponential density distribution, explicit formulas in the literature have only been given for three other density profiles: a linear density distribution $A(x) = -C_0 x$ [22, 23]^{*},

$$(P_c)_{(\text{lin})} = \exp(-\pi \Delta^2 (C_0)^{-1} \sin^2 2\theta), \quad (4.28)$$

a distribution $A(x) = B_0/x$ [33],

$$(P_c)_{(1/x)} = \frac{\exp(4\pi B_0 \cos^2 \theta) - 1}{\exp(4\pi B_0) - 1}, \quad (4.29)$$

and the hyperbolic tangent distribution [34] $A(x) = A_0[1 - \tanh(x/l)]/2$,

$$(P_c)_{(\text{tanh})} = \frac{\cosh(\pi l A_0) - \cosh(\pi l (\Delta_\infty - \Delta))}{\cosh(\pi l (\Delta_\infty + \Delta)) - \cosh(\pi l (\Delta_\infty - \Delta))}. \quad (4.30)$$

In the last equation Δ_∞ is the value of Δ_m deep inside matter, $\Delta_\infty \equiv \lim_{x \rightarrow \infty} \Delta_m = \sqrt{A_0^2 - 2A_0\Delta \cos 2\theta + \Delta^2}$.

What do these distributions have in common that makes them exactly solvable? One important feature that unites them is that the corresponding differential equations can all be put in the hypergeometric form [35]. We next show more directly that Eqs. (2.24), (4.28), (4.29), and (4.30) are all related to each other and that the first three directly follow from the hyperbolic tangent result.

^{*}Notice that Eq. (4.28) is often written in a form containing a factor of $1/\cos 2\theta$. This is done to express C_0^{-1} in terms of the logarithmic derivative of the density at the resonance. In that form, it may superficially appear that P_c has a singularity at $\theta = \pi/4$. Of course, once the derivative is computed, the factors of $\cos 2\theta$ cancel out. As we have discussed in this paper, the conventional definition of the resonance has little physical meaning for large angles, so there is no good reason for introducing the factor of $1/\cos 2\theta$.

To make this relationship clear, it is useful to show the analogs of Eq. (2.15) for the other three distributions in question. A straightforward calculation yields

$$\left(\frac{\Delta_m}{\dot{\theta}_m}\right)_{(\text{lin})} = -\frac{2\Delta^2 \sin^2 2\theta}{C_0 \sin^3 2\theta_m} \quad (4.31)$$

for the linear distribution,

$$\left(\frac{\Delta_m}{\dot{\theta}_m}\right)_{(1/x)} = -\frac{2B_0 \sin^2 2\theta}{\sin 2\theta_m \sin^2(2\theta_m - 2\theta)} \quad (4.32)$$

for the $1/x$ distribution, and

$$\left(\frac{\Delta_m}{\dot{\theta}_m}\right)_{(\text{tanh})} = \frac{A_0 l \sin 2\theta \sin 2\theta_\infty}{\sin 2\theta_m \sin(2\theta_m - 2\theta) \sin(2\theta_m - 2\theta_\infty)} \quad (4.33)$$

for the hyperbolic tangent distribution (θ_∞ is the value of θ_m deep inside matter, so that $\sin 2\theta_\infty = \Delta \sin 2\theta / \Delta_\infty$).

By inspecting Eqs. (2.15), (4.31), (4.32), and (4.33) one can clearly see the common origin of all four solutions. For the hyperbolic tangent distribution $(\Delta_m/\dot{\theta}_m)^{(\text{tanh})}$ has three simple poles in θ_m on $(0, \pi/2]$, thus representing the most general case of all four. The exponential case is obtained when two of the poles, θ_∞ and $\pi/2$, merge in one double pole, and the $1/x$ case is obtained when the poles θ and θ_∞ merge. Finally, if all three poles merge in one triple pole at 0 ($\pi/2$), one obtains the linear case. Thus, given the result for the hyperbolic tangent distribution, it should be possible to recover the answers for the other three distributions by simply taking appropriate limits.

We first show how the exponential result can be obtained from the one for the hyperbolic tangent. By comparing Eqs. (2.24) and (4.30) we see that we need a large A_0 limit of (4.30), since in this case[†] $\theta_\infty \rightarrow \pi/2$, and also a substitution $l \rightarrow 2r_0$.

$$\begin{aligned} (P_c)_{(\text{tanh})} &\longrightarrow \frac{\exp(\pi l A_0)/2 - \exp(\pi l (\Delta_\infty - \Delta))/2}{\exp(\pi l (\Delta_\infty + \Delta))/2 - \exp(\pi l (\Delta_\infty - \Delta))/2} \\ &= \frac{\exp(\pi l (A_0 - (\Delta_\infty - \Delta))) - 1}{\exp(\pi l (2\Delta)) - 1} \end{aligned}$$

[†]Notice that the product $A_0 \sin 2\theta_\infty$ in the limit of large A_0 approaches a constant value $\Delta \sin 2\theta$.

$$\begin{aligned}
& \longrightarrow \frac{\exp(\pi l(A_0 - A_0(1 - (\Delta/A_0) \cos 2\theta) + \Delta)) - 1}{\exp(\pi l(2\Delta)) - 1} \\
& = \frac{\exp(\pi l\Delta(1 + \cos 2\theta)) - 1}{\exp(\pi l(2\Delta)) - 1} \\
& \longrightarrow \frac{\exp(4\pi r_0\Delta \cos^2 \theta) - 1}{\exp(4\pi r_0\Delta) - 1} = (P_c)_{\text{exp}} \tag{4.34}
\end{aligned}$$

Above we used the fact that for large A_0 $\Delta_m = \sqrt{A_0^2 - 2A_0\Delta \cos 2\theta + \Delta^2} \rightarrow A_0(1 - (\Delta/A_0) \cos 2\theta)$. The physical interpretation of this result is the following. For a fixed Δ and $A_0 \rightarrow \infty$ the part of the neutrino trajectory where adiabaticity is maximally violated occurs at large x , where $A_0[1 + \tanh(x/l)]/2 \rightarrow A_0 \exp(-2x/l) = A_0 \exp(-x/r_0)$. Notice, that A_0 dropped out and the derivation is valid for all Δ and θ .

To obtain the result for the linear profile from that for the exponential, in Eq. (2.15) we take the limit $r_0 \rightarrow \infty$, $\theta \rightarrow 0$, such that the product $2\Delta r_0 \sin^2 2\theta$ approaches a constant value, $2(\tilde{\Delta}^2/C_0) \sin^2 2\tilde{\theta}$. In this limit $\exp(4\pi r_0\Delta \cos^2 \theta) \gg 1$ and $\sin^2 2\theta \rightarrow 4 \sin^2 \tilde{\theta}$, so that

$$\begin{aligned}
(P_c)_{\text{exp}} & = \frac{\exp(4\pi r_0\Delta \cos^2 \theta) - 1}{\exp(2\pi l\Delta) - 1} \longrightarrow \exp(-4\pi r_0\Delta \sin^2 \theta) \\
& \longrightarrow \exp(-\pi(\tilde{\Delta}^2/C_0) \sin^2 2\tilde{\theta}) = (P_c)_{\text{lin}}. \tag{4.35}
\end{aligned}$$

At last, we will show how the result for the $1/x$ distribution follows from that for the hyperbolic tangent distribution. The logic is similar to what was done before: Eq. (4.32) can be obtained from Eq. (4.33) by sending $\theta_\infty \rightarrow \theta_m$ and relabeling $A_0 l \rightarrow 2A_0$; the result for the $1/x$ profile should then be read off from the solution of the differential equation with the profile (4.33). A complication arises because in this case one needs to know the solution of the differential equation *between* $\pi/2$ and θ_∞ , while the known result, Eq. (4.30) describes the solution between θ_m and θ_∞ . The range $[\theta_\infty, \pi/2]$ (and also $[0, \theta]$) correspond to a different matter distribution, $A(x) = A_0[1 + 1/\tanh(x/l)]/2$ (see Appendix A).

This difficulty can be easily resolved and the result in question can be obtained from Eq. (4.30) by appropriate substitutions. The key observation is that in the case of the hyperbolic tangent the differential equation is uniquely specified by the *relative* positions of the three poles of Eq. (4.33) and the factor in the numerator. By shifting the poles such that $\theta \rightarrow 0$, we

can reduce the problem of finding the solution on $[\theta_\infty, \pi/2]$ to the solved case $[\theta, \theta_\infty]$ and use Eq. (4.30).

The details of this procedure can be found in Appendix A. After a straightforward calculation one finds that

$$P'_c = \frac{\cosh\left(\pi l A_0 \frac{\sin 2\theta_\infty}{\sin(2\theta_\infty - 2\theta)}\right) - \cosh\left(\pi l A_0 \left(\frac{\sin 2\theta}{\sin(2\theta_\infty - 2\theta)} - 1\right)\right)}{\cosh\left(\pi l A_0 \left(\frac{\sin 2\theta}{\sin(2\theta_\infty - 2\theta)} + 1\right)\right) - \cosh\left(\pi l A_0 \left(\frac{\sin 2\theta}{\sin(2\theta_\infty - 2\theta)} - 1\right)\right)} = \frac{\cosh(\pi l \Delta) - \cosh(\pi l (\Delta_\infty - A_0))}{\cosh(\pi l (\Delta_\infty + A_0)) - \cosh(\pi l (\Delta_\infty - A_0))} \quad (4.36)$$

From the first form of the expression it is easy to see that the formula satisfies the necessary nonadiabatic limit: $\lim_{l \rightarrow 0} P'_c = \cos^2 \theta$. From the second form it is easy to take the limit which reproduces the formula for the $1/x$ profile. We can achieve $\theta_\infty \rightarrow \theta$ by making Δ large while keeping A_0 fixed. Once again, in this limit $\Delta_\infty \rightarrow \Delta - A \cos 2\theta$ and so

$$\begin{aligned} P'_c &\longrightarrow \frac{\exp(\pi l \Delta) - \exp(\pi l (\Delta_\infty - A_0))}{\exp(\pi l (\Delta_\infty + A_0)) - \exp(\pi l (\Delta_\infty - A_0))} \\ &\longrightarrow \frac{\exp(\pi l (\Delta - \Delta_\infty + A_0)) - 1}{\exp(2\pi l A_0) - 1} \\ &\longrightarrow \frac{\exp(2\pi l A_0 \cos^2 \theta) - 1}{\exp(2\pi l A_0) - 1}. \end{aligned} \quad (4.37)$$

Upon relabeling $A_0 l \rightarrow 2A_0$ we recover Eq. (4.32).

The last result deserves a few comments. It is quite remarkable that the dependence of the jumping probability on the mass-squared splitting and energy completely dropped out at the end. The $1/x$ profile thus represents a rather unique case when the adiabaticity is entirely determined by the density profile. This could have been, of course, anticipated already on the basis of the dimensional analysis. Indeed, in the case of $1/x$ distribution the parameter B_0 is *dimensionless* and thus, together with θ , completely determines the jumping probability.

It is instructive to see how the cancellation happens for small θ and $B_0 \gg 1$. Eq. (4.32) then becomes $P_c = \exp(-4\pi B_0 \theta^2)$. But we can also compute this differently: since for small angles the resonance is narrow, we can use a linear formula $P_c = \exp(-\pi \Delta^2 |dA(x)/dx|_{\text{res}}^{-1} \sin^2 2\theta)$. Since for

$A(x) = B_0/x$ we have $dA(x)/dx = -A(x)^2/B_0$ and at the point of resonance $A(x) = \Delta$, the quantity Δ cancels out of the final result:

$$P_c = \exp(-\pi\Delta^2 4\theta^2 B_0/\Delta^2) = \exp(-4\pi\theta^2 B_0) \quad (4.38)$$

The slope at the resonance point changes exactly to compensate for the change in Δ^2 .

5 Conclusions

In this paper we have discussed several aspects of neutrino evolution in the Sun, with an emphasis on physics relevant to large values of the mixing angle, including values greater than $\pi/4$. We have pointed out how some of the results originally derived for small mixing angles can be modified to be applicable to all values of θ . Such results include the adiabaticity condition and the role played by the resonance in determining where the nonadiabatic jumping between the states takes place. We have formulated analytical criteria for the case of the exponential matter distribution and commented on how these criteria change for the realistic solar profile. Although these results were motivated by the neutrino evolution in the QVO regime, they are useful for a general understanding of neutrino oscillations in matter.

We have also studied a specific question: which part of the solar profile causes matter effects in the QVO regime. It was shown why it would be incorrect to estimate those effects from the slope at the point of maximum nonadiabaticity. It was further explained how a particular property of the exponential profile, a double pole at $\theta_m = \pi/2$ and a simple pole at $\theta_m = \theta$ is responsible for the fact that, in changing from the infinite exponential to the BP2000 solar profile in the QVO regime, the effective parameter r_0 changes by less than a factor of 2.

We have presented the results of accurate numerical calculations, showing how the jumping probability P_c interpolates between the QVO and the standard MSW regimes. An empirical prescription on how to estimate P_c anywhere in this range with only elementary functions was given.

Finally, we have shown that the known analytical solutions for the linear, exponential, and $1/x$ density distributions are particular limits of the result for the hyperbolic tangent. This was especially easy to see using θ_m as an independent variable. In the process of the proof we also obtained an answer for a fifth distribution, $N_e \propto (\coth(x/l) \pm 1)$.

Acknowledgments

I would like to thank Plamen Krastev for many pleasant and enlightening conversations and for pointing out several very important references. I am also grateful to Hitoshi Murayama and John Bahcall for their support. This work was supported by the Keck Foundation and by the Director, Office of Science, Office of High Energy and Nuclear Physics, Division of High Energy Physics of the U.S. Department of Energy under Contracts DE-AC03-76SF00098.

A Derivation of the expression for P_c for the density distribution $A(x) \propto (\coth(x/l) \pm 1)$

As mentioned in Section 4, one of the four matter distributions for which exact expressions for P_c have been obtained is the profile $A(x) = A_0[1 + \tanh(x/l)]/2$. The answer is given by Eq. (4.30) and represents result of solving the differential equation (2.11) in the interval $[\theta, \theta_\infty]$, with $\Delta_m/\dot{\theta}_m$ given by Eq. (4.33). In this Appendix we show how this result can be used to obtain the solution to the same differential equation on the interval $[\theta_\infty, \pi/2]$.

Clearly for any x in the distribution $A(x) = A_0[1 + \tanh(x/l)]/2$ the angle θ_m is constrained between θ and θ_∞ . The range of θ_m $[\theta_\infty, \pi/2]$ corresponds to a different density profile, which everywhere satisfies $A(x) > A_0$. This new profile be found by simple analytical continuation. In the original profile the value of the density $A(x) = C$ occurs at

$$x = \frac{l}{2} \log \frac{C}{A_0 - C}. \quad (\text{A.39})$$

When $C > A_0$ the argument of the logarithm becomes negative. Using the analytical continuation of the logarithm, it can be interpreted as

$$x = \frac{l}{2} \left(\log \frac{C}{|A_0 - C|} + i\pi \right) = \tilde{x} + \frac{i\pi l}{2}. \quad (\text{A.40})$$

Substituting this in the equation for $A(x)$ we find

$$\tilde{A}(\tilde{x}) = A_0[1 + \tanh(\tilde{x}/l + i\pi/2)]/2 = A_0[1 + 1/\tanh(\tilde{x}/l)]/2. \quad (\text{A.41})$$

To obtain the expression for P_c for the distribution (A.41), as a first step in Eq. (4.30) we express the quantities Δ_∞ and Δ_m in terms of the angles θ and θ_m ,

$$(P_c)_{(\tanh)} = \frac{\cosh(\pi l A_0) - \cosh\left(\pi l A_0 \frac{\sin 2\theta_\infty - \sin 2\theta}{\sin(2\theta_\infty - 2\theta)}\right)}{\cosh\left(\pi l A_0 \frac{\sin 2\theta_\infty + \sin 2\theta}{\sin(2\theta_\infty - 2\theta)}\right) - \cosh\left(\pi l A_0 \frac{\sin 2\theta_\infty - \sin 2\theta}{\sin(2\theta_\infty - 2\theta)}\right)}. \quad (\text{A.42})$$

Next we shift $\theta_m \rightarrow \theta_m - \theta$ in Eq. (4.33) such that the pole at θ moves to 0. This reduces the problem to solving the differential equation (4.33) between $\theta'_\infty \equiv \pi/2 - \theta$ and $\theta' \equiv \theta_\infty - \theta$. To complete the change to the primed variables, in the numerator of Eq. (4.33) we substitute $A_0 \sin 2\theta \sin 2\theta_\infty$ by $A'_0 \sin 2\theta' \sin 2\theta'_\infty$, where $A'_0 = A_0 \sin 2\theta_\infty / \sin(2\theta_\infty - 2\theta)$. We then find

$$P'_c = \frac{\cosh(\pi l A'_0) - \cosh\left(\pi l A'_0 \frac{\sin 2\theta'_\infty - \sin 2\theta'}{\sin(2\theta'_\infty - 2\theta')}\right)}{\cosh\left(\pi l A'_0 \frac{\sin 2\theta'_\infty + \sin 2\theta'}{\sin(2\theta'_\infty - 2\theta')}\right) - \cosh\left(\pi l A'_0 \frac{\sin 2\theta'_\infty - \sin 2\theta'}{\sin(2\theta'_\infty - 2\theta')}\right)} = \frac{\cosh\left(\pi l A_0 \frac{\sin 2\theta_\infty}{\sin(2\theta_\infty - 2\theta)}\right) - \cosh\left(\pi l A_0 \left(\frac{\sin 2\theta}{\sin(2\theta_\infty - 2\theta)} - 1\right)\right)}{\cosh\left(\pi l A_0 \left(\frac{\sin 2\theta}{\sin(2\theta_\infty - 2\theta)} + 1\right)\right) - \cosh\left(\pi l A_0 \left(\frac{\sin 2\theta}{\sin(2\theta_\infty - 2\theta)} - 1\right)\right)}. \quad (\text{A.43})$$

This is the answer that is needed in Sect. 4.

One may be interested in the expression for P_c for a distribution $A(x) = A_0[1/\tanh(x/l) - 1]/2$, which has the property that it vanishes in the limit of large x . This can be found by redefining the vacuum value of neutrino oscillation parameters to be Δ_∞ and θ_∞ . Eq. (A.43) can then be rewritten as

$$P'_c = \frac{\cosh(\pi l \Delta) - \cosh(\pi l (\Delta_\infty - A_0))}{\cosh(\pi l (\Delta_\infty + A_0)) - \cosh(\pi l (\Delta_\infty - A_0))}, \quad (\text{A.44})$$

where $\Delta = \sqrt{A_0^2 + 2A_0\Delta_\infty \cos 2\theta_\infty + \Delta_\infty^2}$.

References

- [1] B. T. Cleveland *et al.*, *Astrophys. J.* **496**, 505 (1998).
- [2] GALLEX, W. Hampel *et al.*, *Phys. Lett.* **B447**, 127 (1999).

- [3] SAGE, J. N. Abdurashitov *et al.*, Phys. Rev. **C60**, 055801 (1999), astro-ph/9907113.
- [4] Super-Kamiokande, Y. Fukuda *et al.*, Phys. Rev. Lett. **82**, 1810 (1999), hep-ex/9812009.
- [5] Super-Kamiokande, Y. Fukuda *et al.*, Phys. Rev. Lett. **82**, 2430 (1999), hep-ex/9812011.
- [6] J. N. Bahcall, M. Pinsonneault, and S. Basu, (2000), astro-ph/0010346, <http://www.sns.ias.edu/~jnb>.
- [7] L. Wolfenstein, Phys. Rev. **D17**, 2369 (1978).
- [8] S. P. Mikheev and A. Y. Smirnov, Yad. Fiz. (Sov. J. Nucl. Phys.) **42**, 913 (1985).
- [9] S. P. Mikheev and A. Y. Smirnov, Nuovo Cim. **9C**, 17 (1986).
- [10] J. N. Bahcall, P. I. Krastev, and A. Y. Smirnov, Phys. Rev. **D58**, 096016 (1998), hep-ph/9807216.
- [11] C. Giunti, M. C. Gonzalez-Garcia, and C. Pena-Garay, (2000), hep-ph/0001101.
- [12] A. Friedland, Phys. Rev. Lett. **85**, 936 (2000), hep-ph/0002063.
- [13] G. L. Fogli, E. Lisi, D. Montanino, and A. Palazzo, (2000), hep-ph/0005261.
- [14] A. M. Gago, H. Nunokawa, and R. Zukanovich-Funchal, (2000), hep-ph/0007270.
- [15] M. C. Gonzalez-Garcia and C. Pena-Garay, (2000), hep-ph/0009041.
- [16] Y. Suzuki, talk presented at the 19th International Conference on Neutrino Physics and Astrophysics, Neutrino 2000, Sudbury, Canada, June 16-21, 2000.
- [17] A. de Gouvea, A. Friedland, and H. Murayama, (1999), hep-ph/9910286.
- [18] A. de Gouvea, A. Friedland, and H. Murayama, Phys. Lett. **B490**, 125 (2000), hep-ph/0002064.

- [19] G. L. Fogli, E. Lisi, and D. Montanino, Phys. Rev. **D54**, 2048 (1996), hep-ph/9605273.
- [20] S. P. Mikheev and A. Y. Smirnov, Sov. Phys. JETP **65**, 230 (1987).
- [21] H. A. Bethe, Phys. Rev. Lett. **56**, 1305 (1986).
- [22] W. C. Haxton, Phys. Rev. Lett. **57**, 1271 (1986).
- [23] S. J. Parke, Phys. Rev. Lett. **57**, 1275 (1986).
- [24] T. K. Kuo and J. Pantaleone, Rev. Mod. Phys. **61**, 937 (1989).
- [25] E. K. Akhmedov, (1999), hep-ph/0001264.
- [26] W. C. Haxton, (2000), nucl-th/0004052.
- [27] S. P. Mikheev and A. Y. Smirnov, Sov. Phys. Usp. **30**, 759 (1987).
- [28] M. Narayan and S. U. Sankar, (2000), hep-ph/0004204.
- [29] J. Pantaleone, Phys. Lett. **B251**, 618 (1990).
- [30] S. T. Petcov, Phys. Lett. **B214**, 139 (1988).
- [31] T. Kaneko, *Prog. Theor. Phys.* **78**, 532 (1987); S. Toshev, *Phys. Lett. B* **196**, 170 (1987); M. Ito, T. Kaneko, and M. Nakagawa, *Prog. Theor. Phys.* **79**, 13 (1988) [Erratum **79**, 555 (1988)].
- [32] S. T. Petcov, Phys. Lett. **B200**, 373 (1988).
- [33] T. K. Kuo and J. Pantaleone, Phys. Rev. **D39**, 1930 (1989).
- [34] D. Notzold, Phys. Rev. **D36**, 1625 (1987).
- [35] O. V. Bychuk and V. P. Spiridonov, Mod. Phys. Lett. **A5**, 1007 (1990).